On correlations between "dynamic" (small-strain) and "static" (large-strain) stiffness moduli - an experimental investigation on 19 sands and gravels

T. Wichtmann[i], I. Kimmig[ii] Th. Triantafyllidis[iii]

Abstract: Correlations between "dynamic" (small-strain) and "static" (large-strain) stiffness moduli for sand are examined. Such correlations are often used for a simplified estimation of the dynamic stiffness based on static test data. The small-strain shear modulus $G_{dyn} = G_{max}$ and the small-strain constrained modulus $M_{dyn} = M_{max}$ have been measured in resonant column (RC) tests with additional P-wave measurements. Oedometric compression tests were performed in order to determine the large-strain constrained modulus $M_{stat} = M_{oedo}$, while the large-strain Young's modulus $E_{stat} = E_{50}$ was obtained from the initial stage of the stress-strain-curves measured in drained monotonic triaxial tests, evaluated as a secant stiffness between deviatoric stress $q = 0$ and $q = q_{max}/2$. Experimental data for 19 sands or gravels with specially mixed grain size distribution curves, having different non-plastic fines contents, mean grain sizes and uniformity coefficients, were analyzed. Based on the present data, it is demonstrated that a correlation between M_{max} and M_{oedo} proposed in the literature underestimates the dynamic stiffness of coarse and well-graded granular materials. Consequently, modified correlation diagrams for the relationship $M_{max} \leftrightarrow M_{oedo}$ are proposed in the present paper. Furthermore, correlations between G_{max} and M_{oedo} or E_{50}, respectively, have been also investigated. They enable a direct estimation of dynamic shear modulus based on static test data. In contrast to the correlation diagram currently in use, the range of applicability of the new correlations proposed in this paper is clearly defined.

Keywords: Dynamic (small-strain) stiffness; Static (large-strain) stiffness; Correlations; Resonant column tests; P-wave measurements; Oedometric compression tests; Triaxial tests

1 Introduction

It is well known that soil stiffness decreases with increasing magnitude of strain [1, 7, 8, 10, 14, 15, 20–22, 24–29, 33–35, 37, 38, 43, 48, 49]. In many practical problems dealing with dynamic or cyclic loading (except soil liquefaction problems [18, 19, 23, 36]) the strain amplitudes generated in the soil are relatively small. Furthermore, dynamic measurement techniques like resonant column (RC) tests or wave propagation measurements are frequently applied to determine the small-strain stiffness in the laboratory [3,5–7,11,12,16,28,34,35,47]. Therefore, the stiffness at small strains is often also denoted as "dynamic" stiffness. For the stiffness moduli applied in deformation (e.g. settlement) analysis of foundations, usually oedometric compression or triaxial tests with monotonic loading are conducted. The stiffness moduli resulting from these "static" tests have been found significantly lower than the dynamic stiffness. Initially, this has been attributed to the different loading rates applied in the static and dynamic tests. However, it has been recognized soon that the material response of sand is approximately rate-independent and that those differences are due to the different strain levels.

For the design of foundations subjected to dynamic loading, the small-strain shear modulus G_{max} of the subsoil is a key parameter. For final design calculations in large or important projects it will be usually determined from dynamic measurements in situ, e.g. surface or borehole measurements of the wave velocities. However, for feasibility studies, preliminary design calculations or final design calculations in small projects the small-strain shear modulus is often estimated from empirical formulas, tables or correlations with static stiffness values.

For design engineers in practice it is attractive to estimate the dynamic stiffness based on static stiffness data, because static tests are less elaborate than dynamic ones. While the dynamic experiments are conducted by specialized laboratories only, even small soil mechanics laboratories are usually equipped with devices for oedometric testing. Furthermore, for many locations experienced data for the static stiffness moduli are available. Without any further testing these data can be used to estimate the dynamic stiffness.

A diagram providing a correlation between static and dynamic stiffness moduli is incorporated e.g. in the "Recommendations of the working committee Soil Dynamics" of the German Geotechnical Society (DGGT) [9]. It is shown in Figure 1 (area marked by the dark gray colour). The diagram is entered with the large-strain constrained modulus $M_{stat} = M_{oedo}$ (stiffness on the primary compression line obtained from oedometric compression tests) on the ab-

---

[i] Researcher, Institute of Soil Mechanics and Rock Mechanics, Karlsruhe Institute of Technology, Germany (corresponding author). Email: torsten.wichtmann@kit.edu

[ii] Researcher, Institute of Soil Mechanics and Rock Mechanics, Karlsruhe Institute of Technology, Germany

[iii] Professor and Director of the Institute of Soil Mechanics and Rock Mechanics, Karlsruhe Institute of Technology, Germany

scissa and delivers the ratio between small-strain and large-strain constrained moduli $M_{dyn}/M_{stat} = M_{max}/M_{oedo}$ on the ordinate. The small-strain shear modulus $G_{dyn} = G_{max} = M_{max}(1 - \nu - 2\nu^2)/[2(1-\nu)^2]$ can be obtained with an assumption regarding Poisson's ratio ν. Note, that the indices $\sqcup_{dyn}$ and $\sqcup_{max}$ are equivalent, i.e. both denote the small-strain stiffness. The DGGT diagram is based on the correlation between static and dynamic Young's moduli proposed by Alpan [2]. This original correlation is also presented in Figure 1 (black solid curve). Benz & Vermeer [4] have proposed another correlation between static and dynamic constrained moduli (see the area marked by the light gray colour in Figure 1). It is also based on Alpan [2], but in comparison to [9] different assumptions were used when converting the E data into a diagram in terms of M. However, the experimental basis and the range of applicability of all correlations shown in Figure 1 is not clear [4, 45, 46].
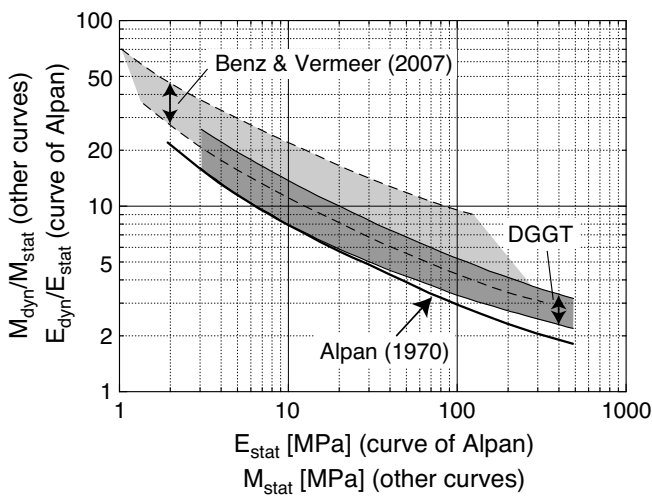
Fig. 1: *Correlation between M_{dyn} and M_{stat} according to the "Recommendations of the working committee Soil Dynamics" of the German Geotechnical Society (DGGT) [9] versus correlation proposed by Benz & Vermeer [4]. The original relationship between E_{dyn} and E_{stat} according to Alpan [2] is also shown.*

A first inspection of the correlations in Figure 1 for four sands with different grain size distribution curves has been presented in [44, 46]. It has been found that the dynamic stiffness of a coarse and a well-graded granular material was significantly underestimated by the range of the DGGT correlation. In consideration of the fact that this correlation is frequently used in practice (at least in Germany), it has been decided to undertake a closer inspection, based on experimental data collected for a wider range of grain size distribution curves. The present paper reports on that new study.

2   Tested materials

The grain size distribution curves of the specially mixed sands or gravels tested in the present study are shown in Figure 2. These are the same mixtures that have been already investigated in [39–43]. The raw material is a natural fluvially deposited quartz sand obtained from a sand pit near Dorsten, Germany, which has been decomposed into 25 gradations with grain sizes between 0.063 mm and 16 mm. The grains have a subangular shape and the grain density is $\varrho_s = 2.65$ g/cm³.

(Figure 2a) have the same uniformity coefficient $C_u = 1.5$ but different mean grain sizes in the range 0.1 mm $\leq d_{50} \leq$ 6 mm. The materials L4 and L10 to L16 (Figure 2b) have the same mean grain size $d_{50} = 0.6$ mm but different uniformity coefficients $1.5 \leq C_u \leq 8$. The inclination of the grain size distribution curve of the fine sands F2 and F4 to F6 (Figure 2a) is similar to that of L1 ($C_u = 1.5$) but these sands contain between 4.4 and 19.6 % silty fines (quartz powder). The sands F1 and F3 have not been tested in the present study but the numbering of the sands chosen in [39] has been maintained herein. The index properties of all tested materials are summarized in Table 1.
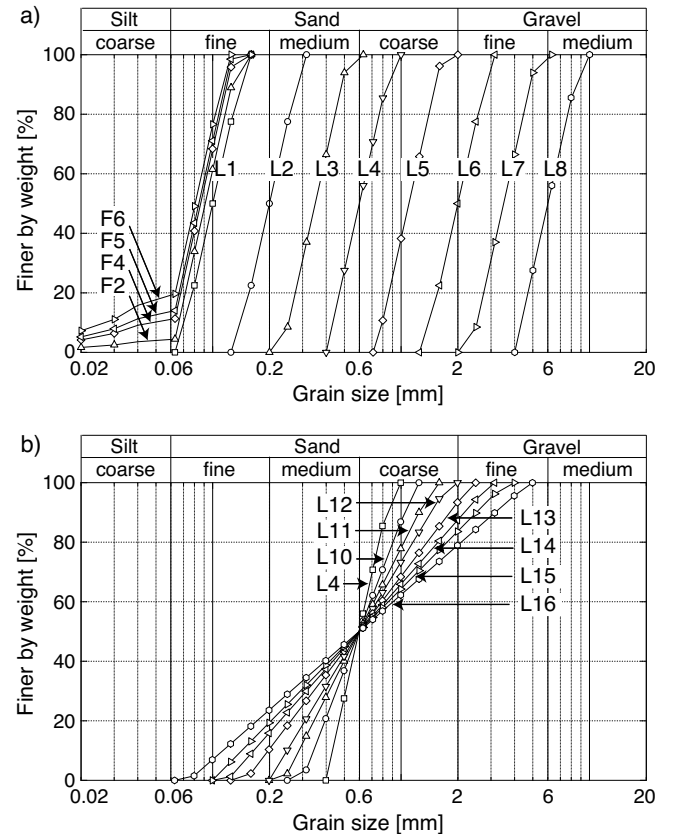
Fig. 2: *Tested grain size distribution curves*

3   Small-strain stiffness from RC tests with additional P-wave measurements

The small-strain stiffness moduli G_{max} and M_{max} were obtained from resonant column tests with additional P-wave measurements, using piezoelectric elements integrated into the end plates of the RC device. The test device, the testing procedure and the test results are documented in detail in [39, 41–43]. The strain level associated with these measurements is about 10^{-6}. For each sand, several samples (diameter $d = 100$ mm, height $h = 200$ mm) with different initial relative densities $D_{r0} = (e_{max} - e_0)/(e_{max} - e_{min})$ were prepared by dry air pluviation and tested in the dry condition at various pressures. Figure 3 shows exemplary data $G_{max}(e, p)$ and $M_{max}(e, p)$ for sand L12. Similar diagrams for the other tested sands can be found in [41, 42]. The increase of G_{max} and M_{max} with decreasing void ratio e and increasing mean pressure p is evident in Figure 3. In case of the coarsest tested material L8, $G_{max}(e, p)$ data

Mat.	FC [%]	d_{50} [mm]	C_u [-]	$e_{\min}$ [-]	$e_{\max}$ [-]
L1	0	0.1	1.5	0.634	1.127
L2	0	0.2	1.5	0.596	0.994
L3	0	0.35	1.5	0.591	0.931
L4	0	0.6	1.5	0.571	0.891
L5	0	1.1	1.5	0.580	0.879
L6	0	2.0	1.5	0.591	0.877
L7	0	3.5	1.5	0.626	0.817
L8	0	6.0	1.5	0.634	0.799
L10	0	0.6	2	0.541	0.864
L11	0	0.6	2.5	0.495	0.856
L12	0	0.6	3	0.474	0.829
L13	0	0.6	4	0.414	0.791
L14	0	0.6	5	0.394	0.749
L15	0	0.6	6	0.387	0.719
L16	0	0.6	8	0.356	0.673
F2	4.4	0.092	1.5	0.734	1.107
F4	11.3	0.086	1.9	0.726	1.117
F5	14.0	0.084	2.6	0.723	1.174
F6	19.6	0.082	3.3	0.746	1.091

Table 1: Index properties (non-plastic fines content FC, mean grain size d_{50}, uniformity coefficient $C_u = d_{60}/d_{10}$, minimum and maximum void ratios $e_{\min}$, $e_{\max}$) of the tested granular materials.

are available, but P-wave measurements were not successful [42], i.e. no $M_{\max}(e,p)$ data exist.

For each granular material, the data of the small-strain shear modulus $G_{\max}(e,p)$ and the small-strain constrained modulus $M_{\max}(e,p)$ have been approximated by the following equations going back to [13, 16]:

$$G_{\max} = A_{Gd} \frac{(a_{Gd} - e)^2}{1 + e} \left(\frac{p}{p_{\mathrm{atm}}}\right)^{n_{Gd}} p_{\mathrm{atm}} \qquad (1)$$

$$M_{\max} = A_{Md} \frac{(a_{Md} - e)^2}{1 + e} \left(\frac{p}{p_{\mathrm{atm}}}\right)^{n_{Md}} p_{\mathrm{atm}} \qquad (2)$$

with atmospheric pressure $p_{\mathrm{atm}} = 100$ kPa. The optimum parameters A_{Gd}, a_{Gd} and n_{Gd} of Eq. (1) as well as A_{Md}, a_{Md} and n_{Md} of Eq. (2) are collected in columns 2 - 7 of Table 2. The notation of these parameters (and similar ones in the following) has been chosen in such way that the first index (G, M, E) denotes the type of stiffness and the second one (d, s) stands for dynamic or static. The solid curves in Figure 3 represent the best fits of Eqs. (1) or (2) to the data of each individual pressure, while the dashed curves are generated using Eqs. (1) or (2) with the parameters given in columns 2 - 7 of Table 2.

In the RC tests, for constant values of void ratio and pressure, $G_{\max}$ and $M_{\max}$ were found to be rather independent of the mean grain size d_{50} of the test material (see $G_{\max}$ data in Figure 4a,b). The only exception is the coarsest tested material L8, where the slightly lower $G_{\max}$ values were presumably caused by an insufficient interlocking between the grains and the end plates of the RC device [41]. In contrast to the d_{50} independence, both small-strain stiffness values were significantly reduced when the uniformity coefficient C_u and the content of non-plastic fines FC increased (Figure 4c-f). A micromechanical explanation of the observed trends of $G_{\max}$ and $M_{\max}$ with C_u and FC based on contact stiffness [17,30] and force transition chains in monodisperse and polydisperse materials [31, 32] is pro-
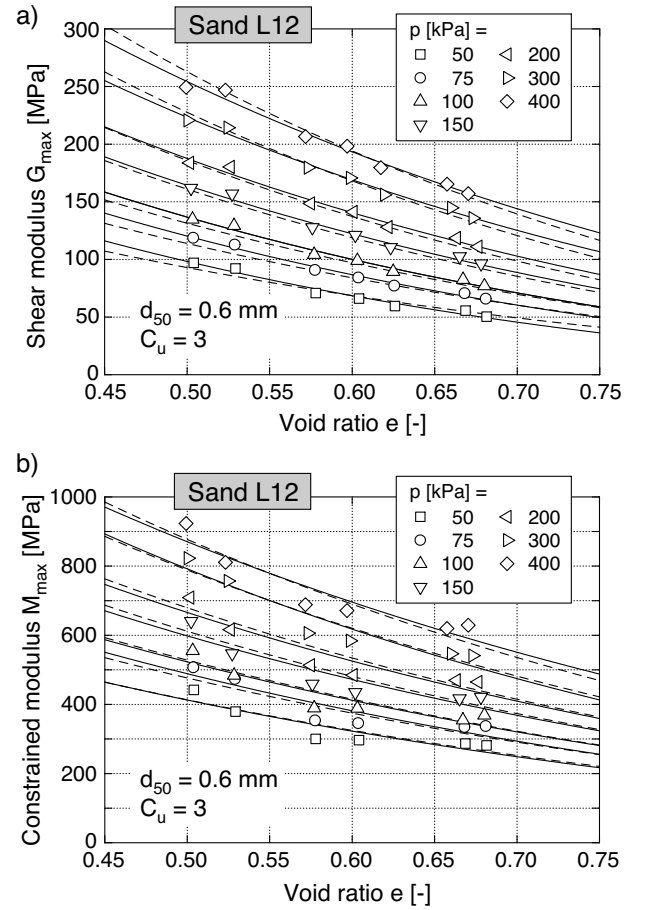
Fig. 3: a) Small strain shear modulus $G_{\max}(e,p)$ and b) small-strain constrained modulus $M_{\max}(e,p)$ measured in the RC tests with additional P-wave measurements on sand L12 (solid curves = best fit of Eqs. (1) or (2) to the data of the individual pressure steps, dashed curves = prediction of Eqs. (1) or (2) with parameters in columns 2 - 7 of Table 2)

vided in [39,41]. In [39,41,42] correlations of the parameters of Eqs. (1) or (2) with the granulometry have been proposed. They can be used for an estimation of small-strain stiffness considering the grain size distribution curve. The estimation via static stiffness values described in this paper is an alternative.

4 Large-strain constrained modulus $M_{\mathbf{oedo}}$ from oedometric compression tests

All sands were tested in oedometric compression tests. The samples were prepared by air pluviation and tested in the dry condition. Different sample dimensions were used:

- Geometry I: diameter $d = 100$ mm, height $h = 18$ mm, $d/h = 5.6$ (used for tests on sands L1 - L3)

- Geometry II: $d = 150$ mm, $h = 30$ mm, $d/h = 5.0$ (used for L1 - L6, L10 - L16, F2, F4 - F6)

- Geometry III: $d = 280$ mm, $h = 80$ mm, $d/h = 3.8$ (used for L2 - L8, L10 - L16)

Most clean sands (L1 - L6, L10 - L16) were tested with two or three different specimen dimensions for comparison purpose. In the case of the largest tested geometry III two tests with loose and two other tests with dense specimens
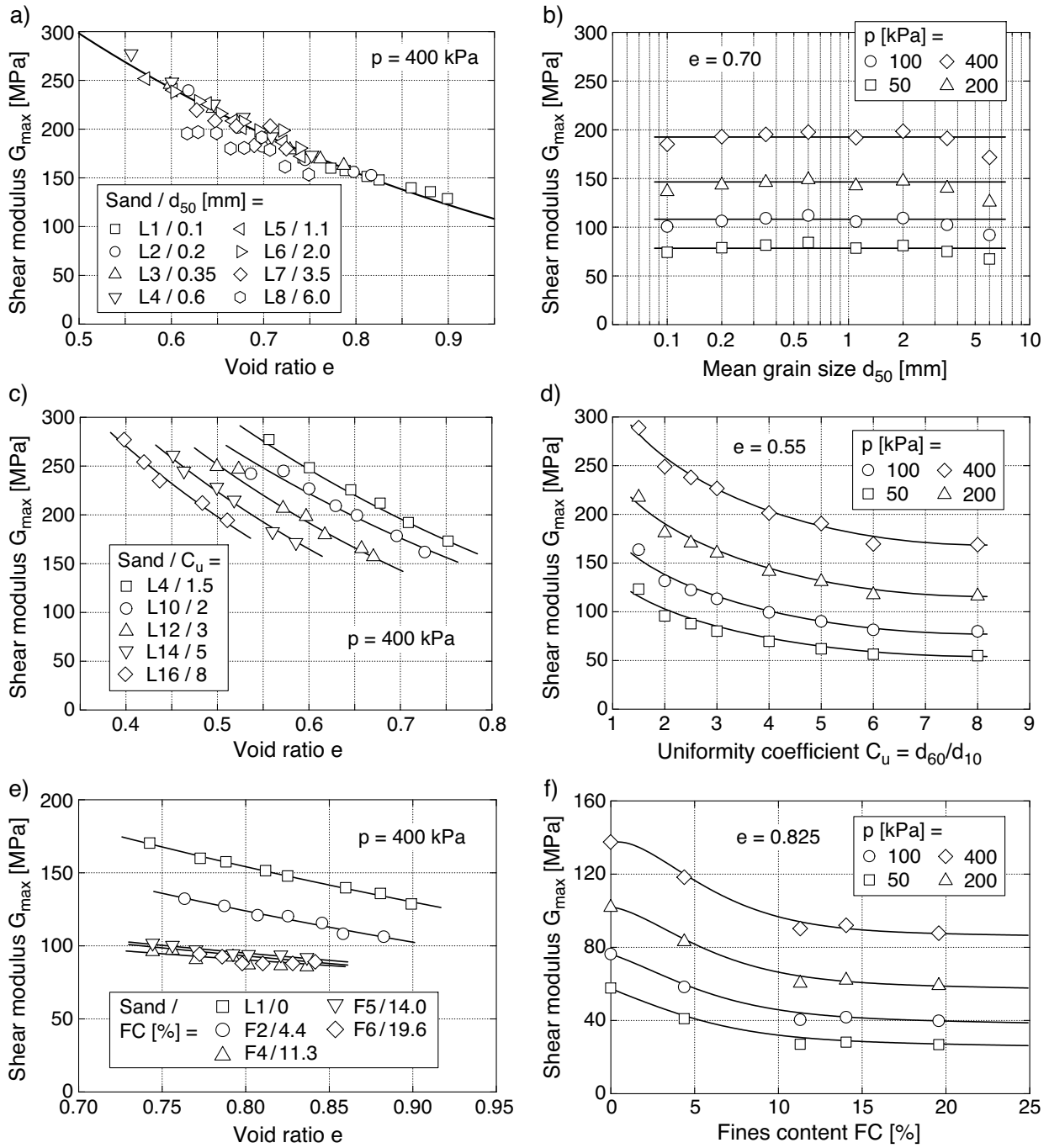
Fig. 4: Small-strain shear modulus G_{max} from resonant column tests a,b) does not depend on mean grain size d_{50} but decreases with c,d) uniformity coefficient C_u and e,f) fines content FC (adapted from [39, 41, 42])

have been performed. In the tests with both smaller sample geometries I and II several samples with various initial densities between loose and dense were tested. Owed to different loading devices the maximum axial stress was $\sigma_1^{max} \approx$ 900 kPa in the case of geometry I, 400 kPa for II and 800 kPa for III.

In each oedometric compression test the axial load has been increased to the maximum vertical stress σ_1^{max}, followed by an unloading to $\sigma_1 = 0$ and a final reloading to σ_1^{max}. Typical curves of void ratio or axial strain versus axial stress from tests with geometry III are given in Figure 5. The constrained modulus M_{oedo} has been derived from the compression curve measured during the first loading to

σ_1^{max}. The un- and reloading curves are not further used in this paper. M_{oedo} is calculated with the increments of axial stress $\Delta\sigma_1$ and void ratio Δe and with the void ratio e_0 at the beginning of a load step:

$$M_{oedo} = \frac{\Delta\sigma_1}{\Delta\varepsilon_1} = \frac{\Delta\sigma_1}{\Delta e}(1 + e_0) \qquad (3)$$

Alternatively, it can be obtained from $M_{oedo} = [\ln(10)(1 + e_0)\sigma_1]/C_c$ with C_c being the actual inclination of the compression curve in a e-log σ_1 diagram at the actual axial stress σ_1. The stiffness M_{oedo} has been evaluated for the same values of mean pressure $p = (\sigma_1 + 2\sigma_3)/3$ that have been used in the RC tests ($p = 50, 75, 100, 150, 200$ and

1	2	3	4	5	6	7	8	9	10	11	12	13	14
Mat.	G_{max}, Eq. (1)			M_{max}, Eq. (2)			M_{oedo}, Eqs. (4) + (5)				E_{50}, Eq. (6)		
	A_{Gd}	a_{Gd}	n_{Gd}	A_{Md}	a_{Md}	n_{Md}	A_{Ms}	$a_{1,Ms}$	$a_{2,Ms}$	n_{Ms}	A_{Es}	a_{Es}	n_{Es}
L1	636	2.34	0.44	547	3.73	0.38	2860	1.37	0.000	0.66	–	–	–
L2	1521	1.79	0.43	3657	1.98	0.37	2320	1.45	0.035	0.59	7500	0.95	0.70
L3	1620	1.77	0.42	3172	2.11	0.35	660	1.90	0.045	0.59	4500	0.95	0.70
L4	2023	1.67	0.41	5804	1.76	0.34	640	1.98	0.080	0.76	5400	0.91	1.00
L5	1570	1.77	0.43	3319	2.05	0.37	1150	1.80	0.100	0.84	4200	0.94	0.88
L6	1035	2.04	0.43	3151	2.10	0.40	300	2.63	0.160	0.81	1000	1.20	0.90
L7	852	2.13	0.45	620	3.80	0.41	850	1.90	0.105	0.80	–	–	–
L8	734	2.16	0.45	–	–	–	350	2.62	0.160	0.75	–	–	–
L10	1207	1.85	0.46	2679	2.20	0.36	1270	1.65	0.075	0.72	–	–	–
L11	2240	1.47	0.48	3280	2.04	0.37	600	1.99	0.100	0.76	–	–	–
L12	2489	1.39	0.50	5512	1.69	0.37	750	1.88	0.110	0.85	5600	0.78	1.00
L13	2969	1.27	0.51	9363	1.40	0.38	730	1.84	0.135	1.06	–	–	–
L14	2771	1.26	0.54	4789	1.72	0.40	470	1.98	0.100	0.86	8000	0.69	0.70
L15	4489	1.08	0.53	10366	1.30	0.40	700	1.76	0.090	0.82	–	–	–
L16	2388	1.27	0.54	17286	1.08	0.42	880	1.54	0.065	0.79	5200	0.68	0.57
F2	571	2.19	0.51	14.7	16.3	0.44	3138	1.32	0.000	0.69	–	–	–
F4	81.6	3.83	0.58	127.7	5.58	0.48	2206	1.32	0.000	0.69	1600	1.13	0.95
F5	71.5	4.09	0.57	170.4	4.97	0.48	1717	1.32	0.000	0.72	–	–	–
F6	17.9	7.19	0.57	132.2	5.39	0.49	2253	1.29	0.000	0.70	2270	1.06	0.84

Table 2: Parameters of Eqs. (1), (2), (4), (5) and (6) for all tested materials

300 kPa). Since the lateral stress could not be measured in the oedometric compression tests, it has been estimated from $\sigma_3 = K_0 \sigma_1$ with $K_0 = 1 - \sin \varphi_P$. The peak friction angle φ_P has been obtained from the drained monotonic triaxial tests (Section 5). Due to the limitations in σ_1^{max}, a mean pressure of $p = 400$ kPa that was applied in the RC tests was not reached in the oedometric compression tests. For $d = 100$ and 280 mm, the attainable pressure was restricted to $p = 300$ kPa, while it was $p = 200$ kPa or even only 150 kPa for $d = 150$ mm (depending on density via $\varphi_P(D_r)$). The axial strains corresponding to the evaluated M_{oedo} values ranged from $\varepsilon_1 = 0.24$ % for the dense sample of L8 at $p = 50$ kPa to $\varepsilon_1 = 5.6$ % for the loose sample of F5 at $p = 150$ kPa (compare also data for L3 in Figure 5b). Therefore, the strains in the oedometric compression tests are about 2,000 to 50,000 times larger than those in the measurements of the small-strain stiffness.

The smallest tested sample geometry ($d = 100$ mm, $h = 18$ mm) was found inappropriate since even for fine sands it delivered significantly lower M_{oedo} values than both other sample dimensions ($d = 150$ mm, $h = 30$ mm and $d = 280$ mm, $h = 80$ mm, see data for L1 and L2 in Figure 6a,b). For uniform fine to medium coarse sands ($d_{50} \leq 2$ mm, $C_u \leq 2.5$) oedometric compression tests with $d = 150$ mm, $h = 30$ mm seem to deliver acceptable results since similar stiffness values as for $d = 280$ mm, $h = 80$ mm were obtained (see data for L2 and L11 in Figure 6b,d). For coarse and well-graded granular materials the largest sample geometry was necessary to collect reliable M_{oedo} data, since the stiffness values for $d = 150$ mm, $h = 30$ mm were found lower than for $d = 280$ mm, $h = 80$ mm (see data for L5, L13 and L15 in Figure 6c,e,f).

The weaker response of the smaller samples probably results from a loosened layer at the top originating from the sample preparation process. The alignment of the upper layer of grains to the load piston during the initial phase of loading may also have contributed to the weaker response. Both influences are larger in case of the samples with lower
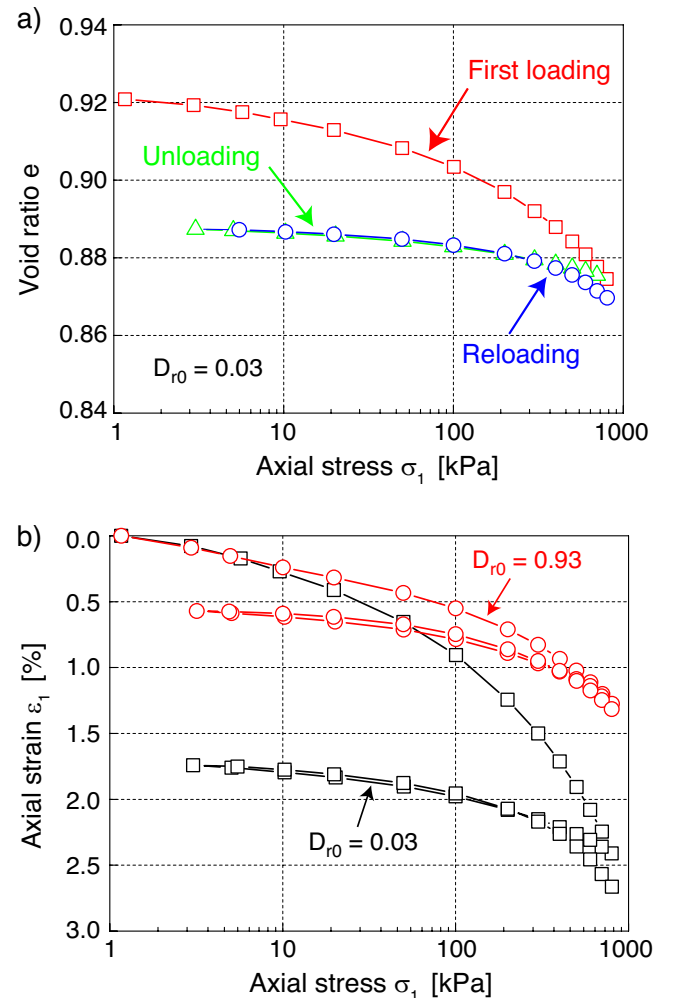
Fig. 5: a) Void ratio and b) axial strain ε_1 versus axial stress in oedometric compression tests on sand L3
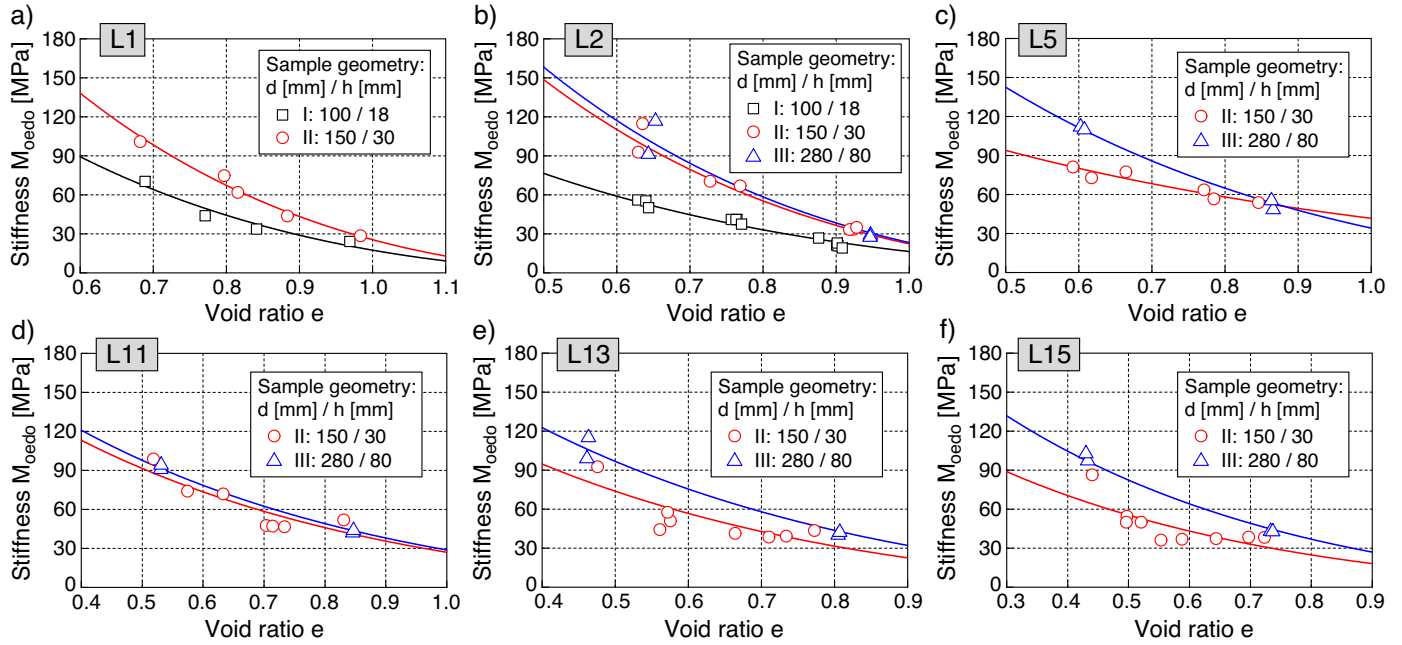
Fig. 6: *Comparison of $M_{oedo}(e)$ data for $p = 150$ kPa obtained from oedometric compression tests with different sample geometries*
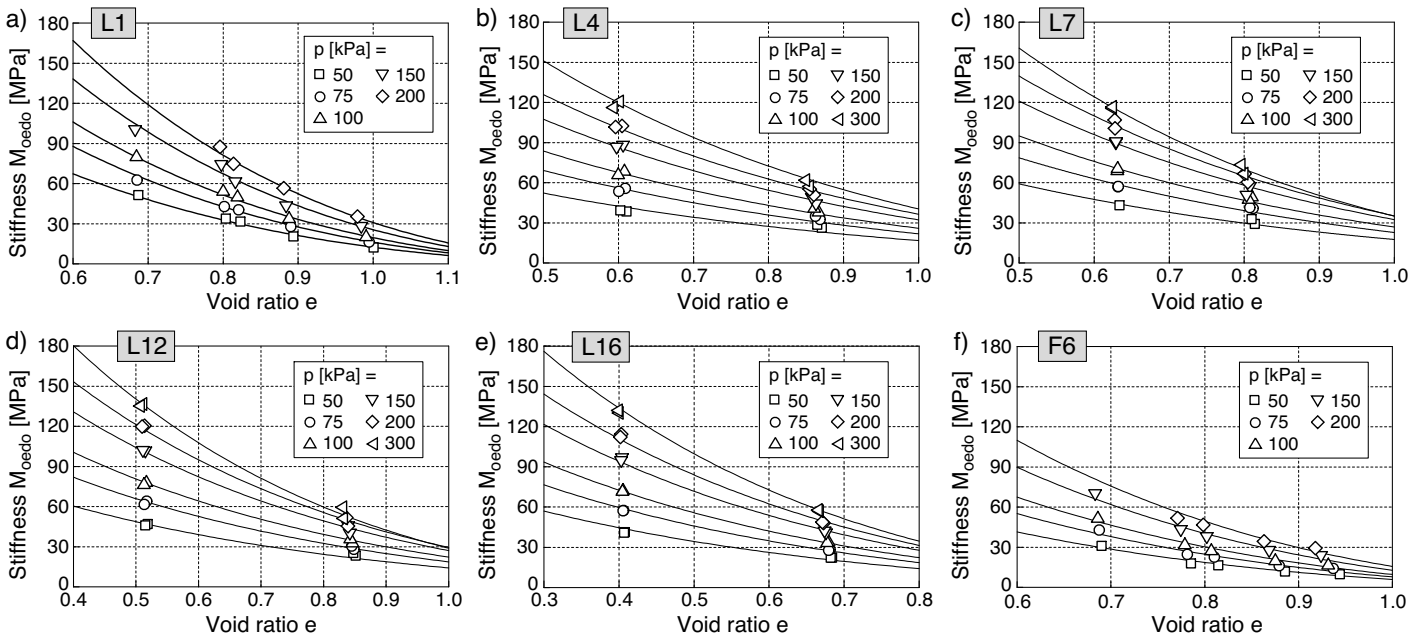
Fig. 7: *$M_{oedo}(e, p)$ data for selected sands, obtained from the oedometric compression tests with the largest tested sample geometry. The black solid curves have been generated using Eqs. (4) and (5) with the parameters given in columns 8 - 11 of Table 2.*

height and become more pronounced if the grain size increases. In contrast, side friction effects seem to be of minor importance. All three tested sample dimensions are in accordance with German standard code DIN 18135 for oedometric testing ($d/h \geq 3$). The ratio of the contact area between the soil and the side wall A_{wall} and the area of the sample cross section A_{sample} increases with increasing sample size. It is $A_{wall}/A_{sample} = 0.72$ for $d = 100$ mm, 0.80 for $d = 150$ mm and 1.14 for $d = 280$ mm. Therefore, the side friction effects will slightly increase with the sample size. The influence on the test data seems, however, to be relatively small since for finer sands (e.g. L2

and L11 in Figure 6) quite similar stiffness values were obtained from the tests with $d = 150$ mm and $d = 280$ mm. Furthermore, if side friction effects were the main reason for the observed geometry influence, then the differences in the stiffness moduli obtained for the different sample geometries should be almost the same for all sands, i.e. the geometry effects should not depend on grain size distribution curve. This is contrasted by the current experimental results.

For the analysis of the correlations with small-strain stiffness values in Section 6, the M_{oedo} data of the largest tested geometry were selected for each sand, i.e. geometry II for
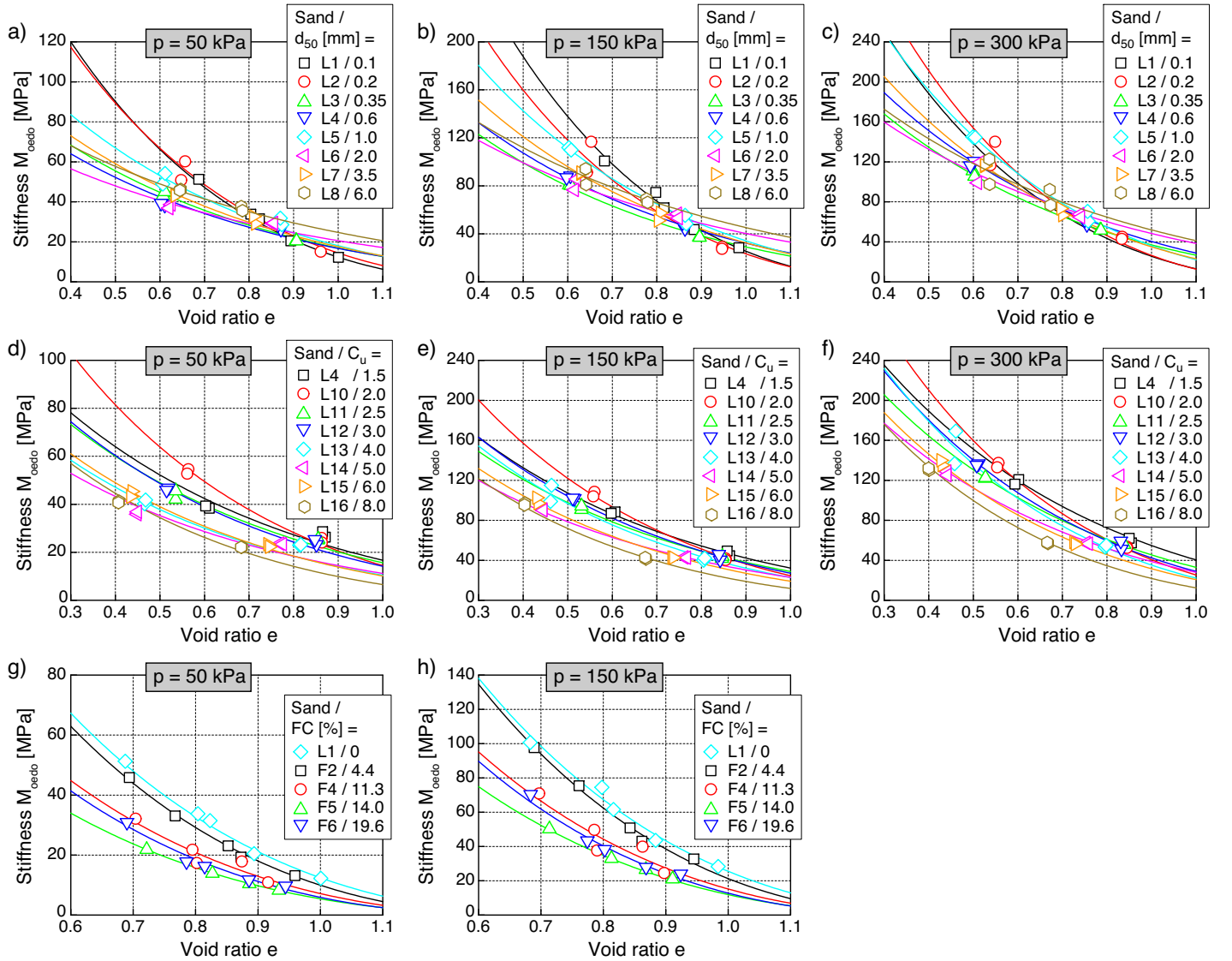
Fig. 8: *Comparison of constrained modulus $M_{oedo}(e)$ for sands with different values of a-c) mean grain size d_{50}, d-f) uniformity coefficient C_u and g-h) fines content FC. Data for three different pressures are provided. Data for $p = 300$ kPa are not available for the sands L1, F2 and F4 - F6 tested with sample dimensions $d = 150$ mm, $h = 30$ mm.*

sands L1, F2 and F4 - F6 and geometry III for all other materials. Figure 7 presents these $M_{oedo}(e,p)$ data for selected sands.

The $M_{oedo}(e,p)$ data of each granular material have been fitted by a slightly modified Eq. (2):

$$M_{oedo} = A_{Ms} \frac{(a_{Ms} - e)^2}{1 + e} \left(\frac{p}{p_{atm}} \right)^{n_{Ms}} p_{atm} \qquad (4)$$

with a parameter a_{Ms} of the void ratio function depending linearly on pressure according to

$$a_{Ms} = a_{1,Ms} - a_{2,Ms} \left(\frac{p}{p_{atm}} \right) \qquad (5)$$

introducing two new material constants $a_{1,Ms}$ and $a_{2,Ms}$. Since the inclination of the curves $M_{oedo}(e)$, i.e. the void ratio dependence of stiffness changes more significantly with pressure than in case of the $G_{max}(e)$ or $M_{max}(e)$ data derived from the RC tests, it was necessary to make the parameter a_{Ms} of Eq. (4) pressure-dependent. The optimum

parameters A_{Ms}, $a_{1,Ms}$, $a_{2,Ms}$ and n_{Ms} for all tested materials are summarized in columns 8 - 11 of Table 2. The prediction of Eq. (4) with these parameters is shown as black solid curves in Figure 7. A value of $a_{2,Ms} = 0$ was usually sufficient for the data from the tests with $d = 150$ mm, i.e. the original Hardin's equation with a constant parameter a in the void ratio function was retrieved.

In Figure 8 the influence of the grain size distribution curve on the M_{oedo} values is inspected for three different pressures $p = 50$, 150 and 300 kPa (data for L1, F2 and F4 - F6 are only available at $p = 50$ and 150 kPa). For constant values of void ratio and pressure, there is no clear tendency concerning the effect of mean grain size d_{50} on M_{oedo} (Figure 8a-c). The only exception are the fine sands L1 and L2 which show a somewhat larger stiffness at low void ratios. Generally, the inclination of the $M_{oedo}(e)$ curves increases with decreasing mean grain size. Despite some scatter of the data, a significant reduction of M_{oedo} with increasing values of uniformity coefficient C_u and fines content FC can be concluded from Figure 8d-h. This is in accordance

with the tendencies measured for the small-strain stiffness moduli G_{max} and M_{max} in the RC tests (Figure 4c-f).

5 Large-strain Young's modulus E_{50} from drained monotonic triaxial tests

Young's modulus E_{50} is obtained from the initial stage of the stress-strain curve measured in drained monotonic triaxial tests. It is evaluated as a secant stiffness for the interval between deviatoric stress $q = 0$ and $q = q_{max}/2$. For all tested materials several drained monotonic triaxial tests with a variation of initial relative density were performed. The effective lateral stress was $\sigma_3' = 100$ kPa in all these tests. All samples ($d = 100$ mm, $h = 100$ mm) were prepared by air pluviation and afterwards saturated with de-aired water. Based on the data of these tests the density-dependent peak friction angle $\varphi_P(D_r)$ used in order to estimate the lateral stress in the oedometric compression tests (see Section 4) has been evaluated. In additional tests on medium dense samples, ten sands (L2 - L6, L12, L14, L16, F4, F6) were also sheared under higher confining stresses $\sigma_3' = 200$ and 400 kPa. Since tests with different confining stresses are necessary to quantify the pressure-dependence of stiffness, only these ten sands are analyzed in the following with respect to $E_{50}(e, p)$. Figure 9 shows typical curves of deviatoric stress q versus axial strain ε_1 measured in two tests with different initial relative densities ($D_{r0} = 0.51$ or 0.87) performed on sand L4. The determination of Young's modulus $E_{50} = \Delta\sigma_1/\Delta\varepsilon_1 = \Delta q/\Delta\varepsilon_1$ from the initial part of the stress-strain curve is also illustrated in Figure 9. The axial strains corresponding to the evaluated E_{50} values ranged from $\varepsilon_1 = 0.5$ % for the dense sample of L4 at $\sigma_3' = 100$ kPa to $\varepsilon_1 = 2.3$ % for the loose sample of L1 at $\sigma_3' = 100$ kPa, being about 5,000 to 20,000 times larger than those corresponding to the small-strain stiffness.
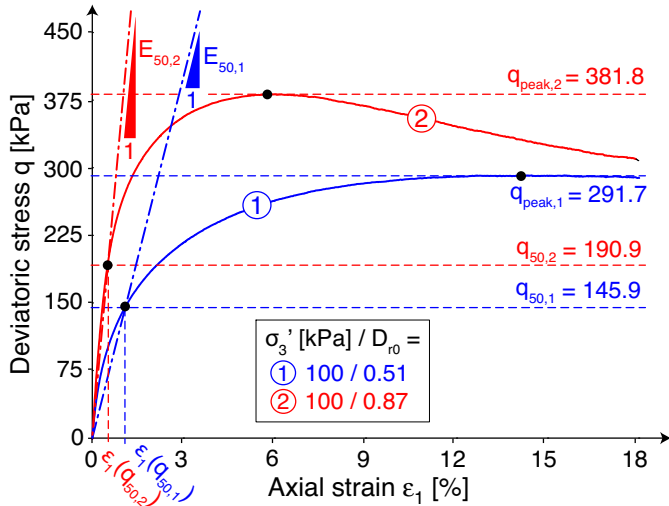
Fig. 9: *Determination of Young's modulus E_{50} from the initial part of the stress-strain curve $q(\varepsilon_1)$ measured in drained monotonic triaxial tests on sand L4*

In Figure 10 the E_{50} data gathered from the triaxial tests are given as a function of void ratio e_{50} or mean pressure p_{50}, respectively. These two quantities are mean values for the piece of the stress-strain curve between $q = 0$ and $q = q_{max}/2$ which has been analyzed with respect to E_{50}. For

each sand the $E_{50}(e_{50}, p_{50})$ data have been fitted by

$$E_{50} = A_{Es}\, \frac{(a_{Es} - e_{50})^2}{1 + e_{50}} \left(\frac{p_{50}}{p_{atm}}\right)^{n_{Es}} p_{atm} \qquad (6)$$

resulting in the parameters A_{Es}, a_{Es} and n_{Es} summarized in columns 12 to 14 of Table 2. The solid curves in Figure 10 represent the prediction of Eq. (6) with these parameters. In the E_{50}-e_{50} diagrams in the upper row of Figure 10, for each sand a mean value of pressure p_{50} from all tests with $\sigma_3' = 100$ kPa has been used for generating these curves, while Eq. (6) was applied with a mean value of void ratio e_{50} in the three tests with different confining stresses in order to plot the lines in the E_{50}-p_{50} diagrams in the lower row of Figure 10.

In the diagrams of Figure 10a,d no clear correlation between E_{50} and mean grain size can be found. For constant values of pressure and void ratio, however, the finest tested sand L2 shows somewhat larger stiffness values than the other uniform materials. In contrast, a significant decrease of Young's modulus with increasing uniformity coefficient for $e_{50} = $ constant is evident in Figure 10b. It is due to the fact that the void ratios are generally lower at higher C_u. Two samples having the same e_{50} may thus be either in the loose or dense state for either high or low C_u values. For example, $e_{50} = 0.5$ means a high density for $C_u = 3.0$ (L12) but a low one for $C_u = 8.0$ (L16). Consequently a much larger Young's modulus is observed for L12 than for L16 at that void ratio. Furthermore, the pressure-dependence of E_{50} gets lower with increasing C_u (Figure 10e), resulting in a decrease of the n_{Es} parameter of Eq. (6) with C_u. This is in contrast to the small-strain stiffness, where the pressure-dependence gets more pronounced with increasing uniformity coefficient [41, 42]. The Young's moduli of the two silty sands F4 and F6 are similar (Figures 10c,f) and of the same magnitude as the E_{50} values of the uniform clean sands L2 to L6 (compare Figures 10a and 10c). Therefore, in contrast to the decrease of the small-strain stiffness with FC (Figure 3e,f), the influence of fines content on Young's modulus E_{50} was found negligible.

6 Correlations between "dynamic" and "static" stiffness

6.1 Correlation between M_{max} and M_{oedo}

For each sand the small-strain (dynamic) constrained modulus M_{max} was calculated from Eq. (2) using the parameters in columns 5 to 7 of Table 2. The large-strain (static) constrained modulus M_{oedo} was obtained from Eqs. (4) and (5) with the constants given in columns 8 to 11 of Table 2. Both stiffness values were evaluated for three different pressures $p = 50$, 150 and 300 kPa and for the range of relative densities $D_{r,min} \le D_r \le D_{r,max}$ that was covered by both the RC and the oedometric compression tests on the given material (see common range in Table 3). The data have been analyzed in steps of $\Delta D_r = (D_{r,max} - D_{r,min})/10$. Afterwards the ratio M_{max}/M_{oedo} of dynamic and static moduli was plotted versus the static values M_{oedo}.

Such data for all tested materials are given in Figure 11a. The remaining three diagrams in Figure 11b-d show the same data but distinguished with respect to the grain size distribution curve. Figure 11b pertains to clean and silty fine sands (materials L1, L2 and F2 to F6 with $d_{50} \le 0.2$ mm and $0 \le FC \le 20$ %), Figure 11c to poorly graded medium coarse sands to fine gravels (materials L3 to L7 and
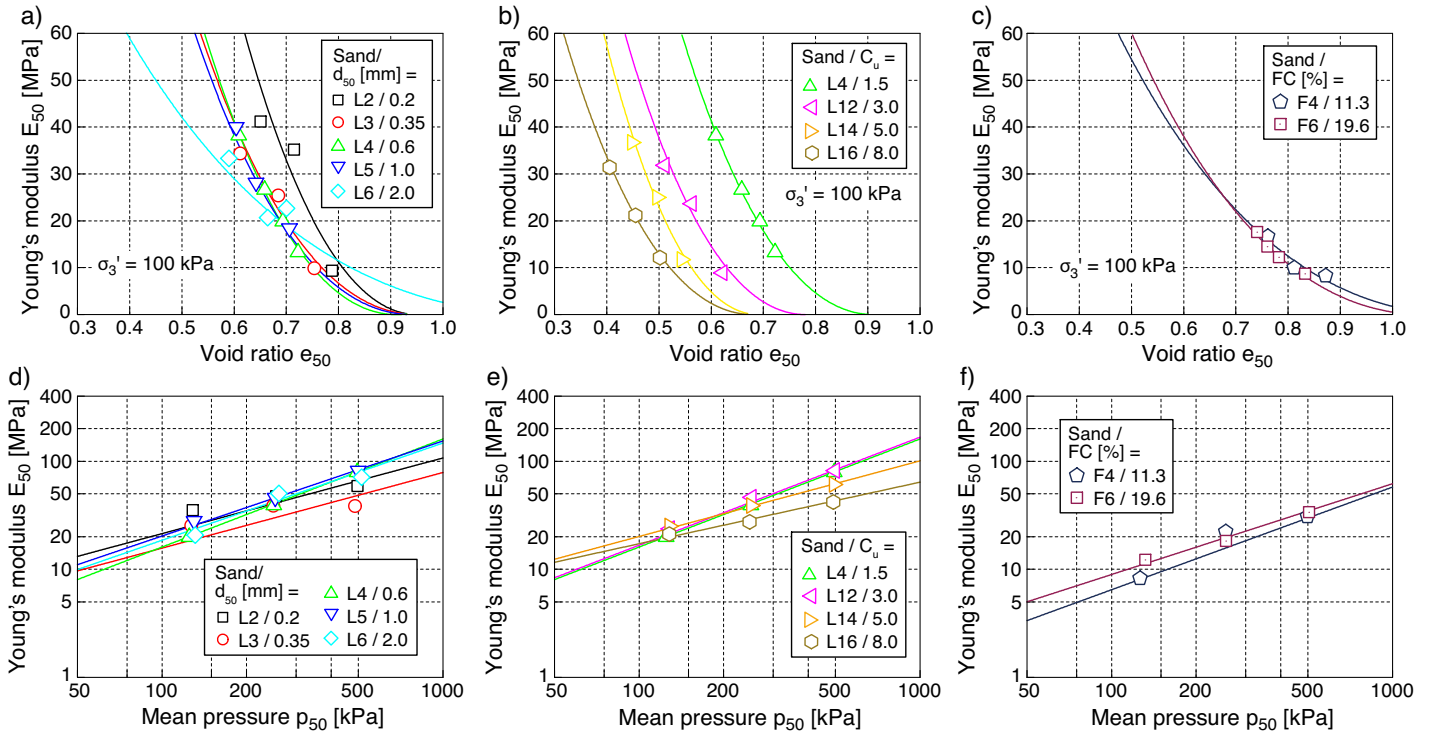
Fig. 10: Young's modulus E_{50} derived from the drained monotonic triaxial tests as a function of void ratio e_{50} (upper row, for $\sigma_3' = 100$ kPa) and mean pressure p_{50} (lower row, for medium density). The solid curves have been generated with Eq. (6) and the constants in columns 12 to 14 of Table 2.

| Mat. | Correlations M_{max}/M_{oedo}-M_{oedo} and G_{max}/M_{oedo}-M_{oedo} | | | | | | Correlation G_{max}/E_{50}-E_{50} | | | |
| | RC tests | | Oedometric tests | | Common range | | Triaxial tests | | Common range | |
	$D_{r,min}$	$D_{r,max}$	$D_{r,min}$	$D_{r,max}$	$D_{r,min}$	$D_{r,max}$	$D_{r,min}$	$D_{r,max}$	$D_{r,min}$	$D_{r,max}$
L1	0.42	0.78	0.26	0.89	0.42	0.78	-	-	-	-
L2	0.42	0.94	0.08	0.87	0.42	0.87	0.49	0.86	0.49	0.86
L3	0.39	0.98	0.07	0.95	0.39	0.95	0.49	0.93	0.49	0.93
L4	0.53	0.94	0.06	0.90	0.53	0.90	0.51	0.87	0.53	0.87
L5	0.44	1.03	0.02	0.91	0.44	0.91	0.56	0.91	0.56	0.91
L6	0.57	0.95	0.07	0.90	0.57	0.90	0.57	0.95	0.57	0.95
L7	0.43	0.99	0.02	0.96	0.43	0.96	-	-	-	-
L8	0.25	1.10	0.08	0.93	0.25	0.93	-	-	-	-
L10	0.41	1.01	0.00	0.94	0.41	0.94	-	-	-	-
L11	0.43	0.93	0.01	0.90	0.43	0.90	-	-	-	-
L12	0.42	0.93	-0.05	0.89	0.42	0.89	0.55	0.89	0.55	0.89
L13	0.44	0.87	-0.07	0.86	0.44	0.86	-	-	-	-
L14	0.43	0.84	-0.06	0.85	0.43	0.84	0.56	0.84	0.56	0.84
L15	0.51	0.86	-0.08	0.86	0.51	0.86	-	-	-	-
L16	0.48	0.87	-0.03	0.84	0.48	0.84	0.51	0.83	0.51	0.83
F2	0.54	0.92	0.40	1.11	0.54	0.92	-	-	-	-
F4	0.54	0.90	0.51	1.06	0.54	0.90	0.59	0.89	0.59	0.89
F5	0.68	0.95	0.53	1.00	0.68	0.95	-	-	-	-
F6	0.63	0.92	0.43	1.16	0.63	0.92	0.71	1.00	0.71	0.92

Table 3: Range of relative densities $D_{r,min} \leq D_r \leq D_{r,max}$ tested in the RC, oedometric compression or drained monotonic triaxial tests and common ranges for the analysis of the various correlations

L10 with 0.35 mm $\leq d_{50} \leq$ 3.5 mm and $1.5 \leq C_u \leq 2.0$) and Figure 11d to more well-graded clean sands (materials L11 to L16 with $d_{50} = 0.6$ mm and $2.5 \leq C_u \leq 8$). Note that no data for L8 are provided in Figure 11 because no $M_{\max}(e, p)$ data are available for that material.

The relationships between $M_{\max}/M_{\mathrm{oedo}}$ and M_{oedo} shown in Figure 11 depend on pressure. Higher pressures mean larger static stiffness values M_{oedo} and lower stiffness ratios $M_{\max}/M_{\mathrm{oedo}}$, which agrees well with the tendency of the correlations provided in Figure 1. The influence of density on the curves in the $M_{\max}/M_{\mathrm{oedo}}$-$M_{\mathrm{oedo}}$ diagrams, however, depends on the grain size distribution curve. For constant values of pressure, a higher density of course corresponds to larger M_{oedo} values. The ratio $M_{\max}/M_{\mathrm{oedo}}$, however, may either increase or decrease with increasing D_r. A reduction of $M_{\max}/M_{\mathrm{oedo}}$ with increasing M_{oedo} (i.e. increasing density) was found for most of the uniform sands and gravels with or without fines, which again is in accordance with the trend of the correlations from the literature (Figure 1). The opposite tendency, however, was observed for the more well-graded granular materials. The different inclinations of the $M_{\max}/M_{\mathrm{oedo}}$-$M_{\mathrm{oedo}}$ curves are connected with the a parameters in Eqs. (2) and (4), describing the void ratio dependence of the small-strain or large-strain stiffness, respectively. While $a_{1,Ms}$ for M_{oedo} is only slightly affected by the grain size distribution curve (see Table 2, somewhat lower $a_{1,Ms}$ values were observed for the finer sands, while $a_{1,Ms}$ is rather independent of C_u), the variation of a_{Md} for $M_{\max}$ with granulometry is much more pronounced. The parameter a_{Md} decreases with C_u and strongly grows with the fines content (Table 2). A larger a_{Md} value means a less pronounced void ratio dependence of the small-strain stiffness. Keeping $a_{1,Ms}$ constant, low values of a_{Md} lead to a positive inclination of the $M_{\max}/M_{\mathrm{oedo}}$-$M_{\mathrm{oedo}}$ curves (as in case of the more well-graded sands in Figure 11d) while the opposite tendency is obtained for high a_{Md} values (see the data for the silty and clean fine sands in Figure 11b).

The ranges of the correlations shown in Figure 1 have been also added in the diagrams of Figure 11. While the correlation recommended by DGGT [9] fits well for clean and silty fine sands (Figure 11b), it underestimates the dynamic stiffness of coarse (Figure 11c) and well-graded (Figure 11d) granular materials. Therefore, the conclusions of the earlier investigation documented in [44, 46] were confirmed. The range of the correlation proposed by Benz & Vermeer [4] encompasses the data for the coarse and well-graded granular materials (Figure 11c,d), but most of the data for clean and silty fine sands fall below that range (Figure 11b). It can be concluded that none of the correlations proposed in the literature covers the whole range of $M_{\max}/M_{\mathrm{oedo}}$ - M_{oedo} data collected in the present study for the various tested grain size distribution curves.

The correlations derived from the data of the present study have been summarized in Figure 11e. For simplicity reasons, the ranges for clean sands from Figures 11c and Figure 11d have been summarized because they were almost congruent. Therefore, the diagram provides a correlation for clean and silty uniform fine sands ($d_{50} \leq 0.2$ mm, $0 \% \leq FC \leq 20 \%$) and another one for coarser and more well-graded clean sands (0.35 mm $\leq d_{50} \leq 3.5$ mm and $2.5 \leq C_u \leq 8$). These correlations are recommended for a more reliable estimation of $M_{\max}/M_{\mathrm{oedo}}$ in practice, considering

the grain size distribution curve of a given granular material. In contrast to the relationships collected in Figure 1, the range of applicability (mean pressures 50 kPa $\leq p \leq$ 300 kPa, relative densities about $0.4 \leq D_r \leq 0.9$) of the new correlations shown in Figure 11e is clearly defined.

6.2 Correlation between $G_{\max}$ and $M_{\mathbf{oedo}}$
For the design of foundations under dynamic loading, usually the shear modulus $G_{\max}$ and not $M_{\max}$ is needed. If correlation diagrams as those in Figure 11 are applied, an assumption concerning Poisson's ratio ν is necessary in order to convert $M_{\max}$ to $G_{\max}$. A direct correlation between $G_{\max}$ and M_{oedo} would be advantageous since it makes such assumption dispensable.

In order to derive such a direct correlation, the dynamic shear modulus $G_{\max}$ was calculated from Eq. (1) using the constants given in columns 2 to 4 of Table 2. The M_{oedo} data were already known from the analysis presented in Section 6.1. In Figure 12 the ratio $G_{\max}/M_{\mathrm{oedo}}$ is plotted versus M_{oedo}. Figure 12a presents the data of all tested materials, Figure 12b those of all clean sands and gravels (0.1 mm $\leq d_{50} \leq$ 6 mm, $1.5 \leq C_u \leq 8$, including also data for L8) and Figure 12c the values for the silty fine sands F2 - F6. Evidently, for a given material the $G_{\max}/M_{\mathrm{oedo}}$-$M_{\mathrm{oedo}}$ curves in Figure 12 show the same tendencies as the $M_{\max}/M_{\mathrm{oedo}}$-$M_{\mathrm{oedo}}$ relationships in Figure 11. Again, the stiffness ratios determined for the clean granular materials lie above those evaluated for the fine sands possessing a certain amount of non-plastic fines. Based on Figure 12b,c, Figure 12d presents a correlation diagram recommended for a practical application based on the current experimental study, distinguishing between clean sands and silty fine sands.

6.3 Correlation between $G_{\max}$ and E_{50}
A correlation between $G_{\max}$ and E_{50} from the drained monotonic triaxial tests has been also established, based on the Young's moduli calculated from Eq. (6) with the parameters in columns 12 to 14 of Table 2. The correlation has been evaluated for all ten sands for which $E_{50}(e, p)$ data were available, and for the common ranges of D_r values from the RC and the triaxial tests (Table 3). Figure 13a contains the data for all sands, while the diagrams in Figure 13b,c distinguish between the clean sands L2 - L16 (Figure 13b) and the silty sands F2 and F4 (Figure 13c). For all tested sands and a given pressure, the ratio $G_{\max}/E_{50}$ decreases with increasing values of E_{50}. Considering a constant value of E_{50}, the ratio $G_{\max}/E_{50}$ usually grows with increasing pressure. For a given pressure, the range of the stiffness ratios obtained for the various clean sands is similar (Figure 13b), i.e. there is no significant influence of the grain size distribution curve. The $G_{\max}/E_{50}$ values of the silty fine sands lie significantly below those of the clean sands. Therefore, the correlation diagram recommended for a practical application (Figure 13d) distinguishes a range for clean granular materials and another one for silty fine sands. The correlation shown in Figure 13d can be used to estimate the dynamic shear modulus directly from the E_{50} data available from drained monotonic triaxial tests. The pressure-dependence can be considered by choosing the lower range (for low pressures as $p = 50$ kPa), the middle range (for medium pressures as $p = 150$ kPa) or the upper range (for high pressures as $p = 300$ kPa) of the
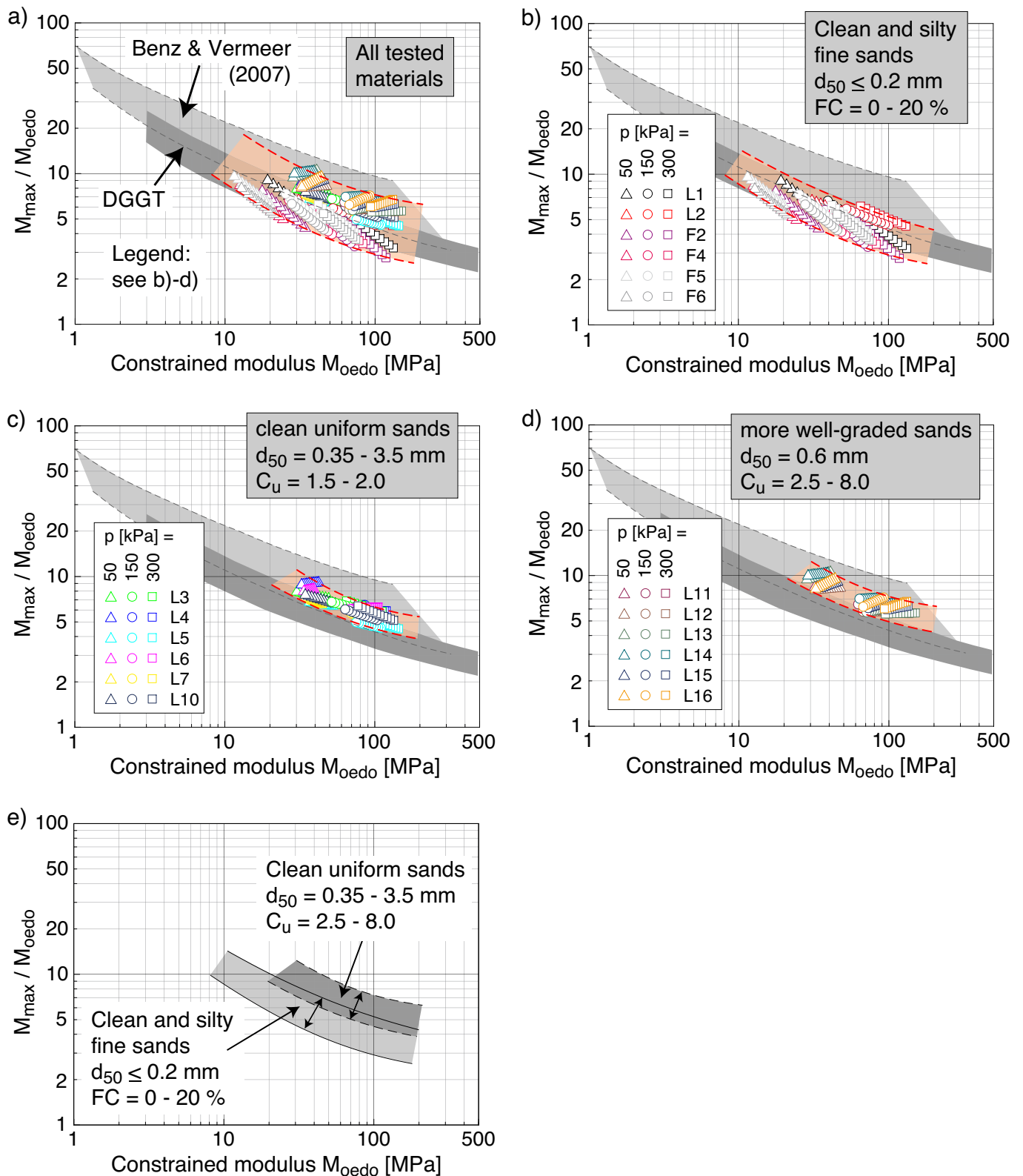
Fig. 11: *Correlation between M_{max}/M_{oedo} and M_{oedo} from oedometric compression tests for a) all tested materials b) clean and silty fine sands, c) clean uniform medium coarse sands to fine gravels, d) more well-graded clean sands; e) correlation diagram proposed for practical application*
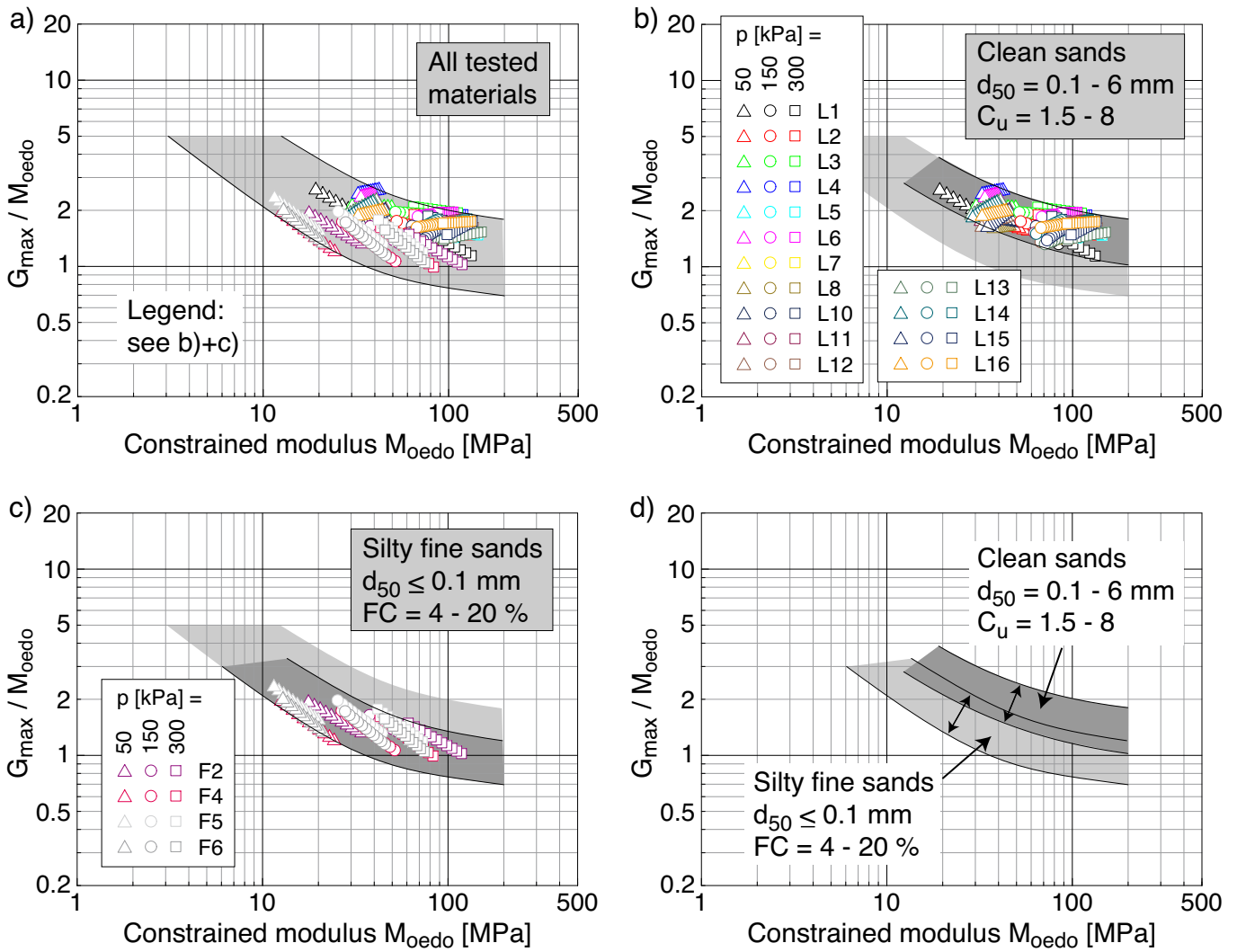
Fig. 12: *Correlation between G_{max}/M_{oedo} and M_{oedo} from oedometric compression tests for a) all tested materials, b) clean sands, c) silty fine sands; d) correlation diagram proposed for practical application*

bandwidths in Figure 13d (compare the pressure influence in Figure 13b-c).

7   Summary and conclusions

Correlations between "dynamic" (small-strain) and "static" (large-strain) stiffness moduli proposed in the literature have been inspected based on the data from resonant column (RC) tests, oedometric compression tests and drained monotonic triaxial tests performed on 19 sands or gravels with specially mixed grain size distribution curves. The small-strain shear modulus $G_{dyn} = G_{max}$ and the small-strain constrained modulus $M_{dyn} = M_{max}$ were obtained from the RC tests with additional P-wave measurements. The data from oedometric compression tests performed with three different sample geometries were evaluated with respect to the large strain constrained modulus $M_{stat} = M_{oedo}$. The smallest tested sample geometry ($d = 100$ mm, $h = 18$ mm) was found inappropriate since even for fine sands it delivered significantly lower M_{oedo} values than both other sample dimensions ($d = 150$ mm, $h = 30$ mm and $d = 280$ mm, $h = 80$ mm). For uniform fine to medium coarse sands oedometric compression tests with $d = 150$ mm, $h = 30$ mm seem to be sufficient

since similar stiffness values as for $d = 280$ mm, $h = 80$ mm were obtained. For coarse and well-graded granular materials the largest sample geometry ($d = 280$ mm, $h = 80$ mm) was necessary to collect reliable M_{oedo} data. For the analysis of the correlations with small-strain stiffness values, the M_{oedo} data for the largest tested geometry were selected for each sand. Beside M_{oedo}, the large-strain Young's modulus $E_{stat} = E_{50}$ was derived from the initial piece of the stress-strain curves $q(\varepsilon_1)$ measured in drained monotonic triaxial tests. Both the small-strain and the large-strain stiffness moduli were evaluated for different pressures (50 kPa $\leq p \leq$ 300 kPa) and relative densities (common range usually about $0.4 \leq D_r \leq 0.9$).

Diagrams showing the stiffness ratio M_{max}/M_{oedo} versus M_{oedo} have been established for each tested material. While the range of the correlation proposed by the DGGT [9] fits well for clean and silty fine sands, it significantly underestimates the dynamic stiffness of coarse and well-graded granular materials. Consequently, based on the data from the present study, a modified correlation diagram showing M_{max}/M_{oedo} versus M_{oedo} considering granulometry has been proposed. Furthermore, alternative correlations between G_{max} and M_{oedo} or E_{50}, respectively, have been also
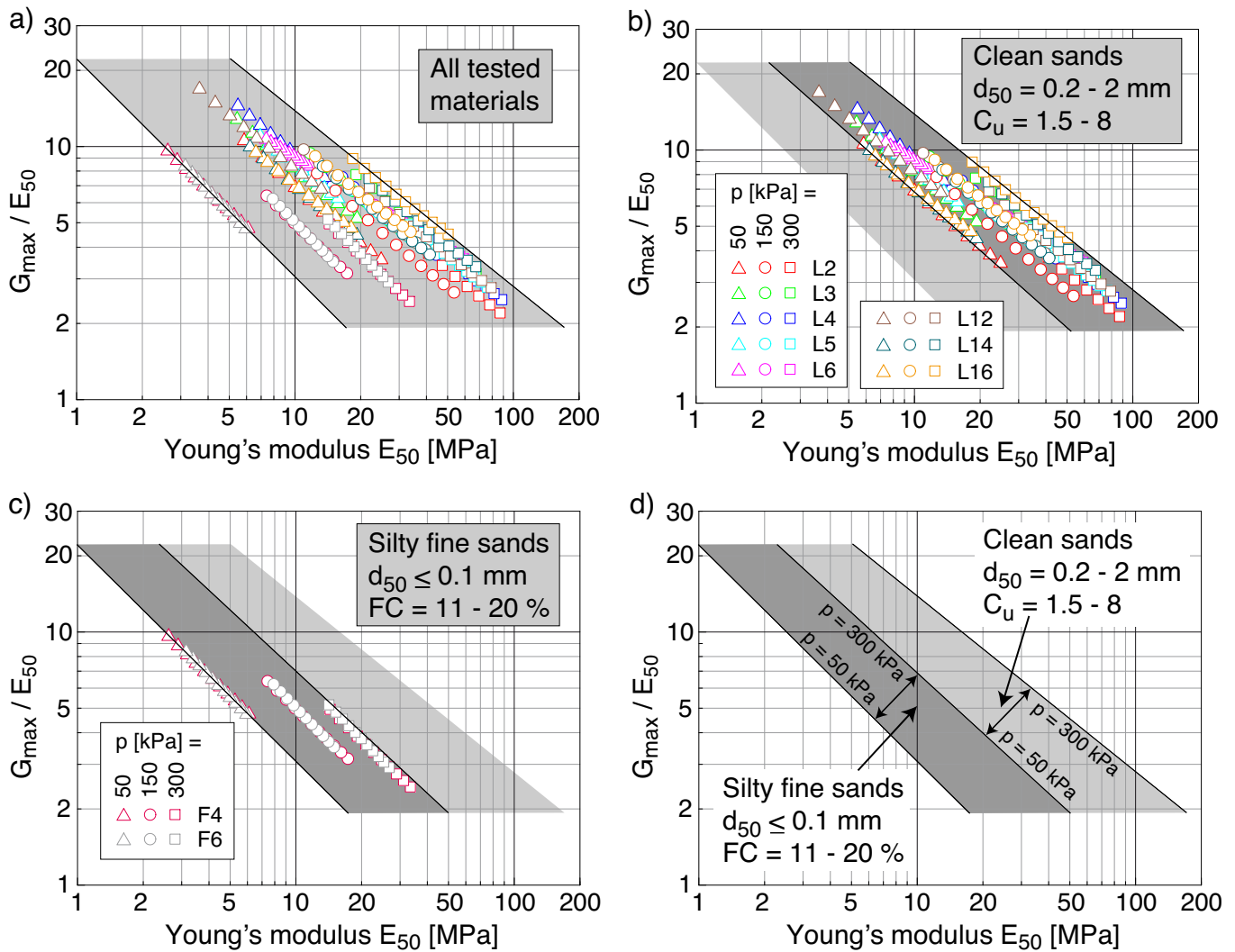
Fig. 13: *Correlation between* G_{max}/E_{50} *and* E_{50} *from drained monotonic triaxial tests for a) all tested materials, b) clean sands, c) silty fine sands; d) correlation diagram proposed for practical application*

developed. They can be used for a direct estimation of the small-strain shear modulus based on oedometric or triaxial test data. Such correlations are of advantage for a practical application since an assumption regarding Poisson's ratio ν is dispensable. In contrast to the available correlations in the literature, the range of applicability of the new correlations ($50 \text{ kPa} \leq p \leq 300 \text{ kPa}$, $0.4 \leq D_r \leq 0.9$) is clearly defined.

Acknowledgements

References

[1] A. Alarcon-Guzman, J.L. Chameau, G.A. Leonardos, and J.D. Frost. Shear modulus and cyclic undrained behavior of sands. *Soils and Foundations*, 29(4):105–119, 1989.

[2] I. Alpan. The Geotechnical Properties of Soils. *Earth Science Reviews, Elsevier*, (6):5–49, 1970.

[3] R. Arulnathan, R.W. Boulanger, and M.F. Riemer. Analysis of bender elements tests. *Geotechnical Testing Journal, ASTM*, 21(2):120–131, 1998.

[4] T. Benz and P.A. Vermeer. Discussion of "On the correlation of oedometric and "dynamic" stiffness of non-cohesive soils" by T. Wichtmann and Th. Triantafyllidis (Bautechnik 83, No. 7, 2006) (in German). *Bautechnik*, 84(5):361–364, 2007.

[5] G.M. Brignoli, M. Gotti, and K.H. II. Stokoe. Measurement of shear waves in laboratory specimens by means of piezo-electric transducers. *Geotechnical Testing Journal, ASTM*, 19(4):384–397, 1996.

[6] S.K. Chaudhary, J. Kuwano, and Y. Hayano. Measurement of quasi-elastic stiffness parameters of dense Toyoura sand in hollow cylinder apparatus and triaxial apparatus with bender elements. *Geotechnical Testing Journal, ASTM*, 27(1):23–35, 2004.

[7] R.M. Chung, F.Y. Yokel, and H. Wechsler. Pore pressure buildup in resonant column tests. *Journal of Geotechnical Engineering, ASCE*, 110(2):247–261, 1984.

[8] C. R. I. Clayton. Stiffness at small strain: research and practice. *Géotechnique*, 61(1):5–37, 2011.

[9] DGGT. Empfehlungen des Arbeitskreises 1.4 "Baugrunddynamik" der Deutschen Gesellschaft für Geotechnik e.V., 2002.

[10] C.S. El Mohtar, V.P. Drnevich, M. Santagata, and A. Bobet. Combined resonant column and cyclic triaxial tests for measuring undrained shear modulus reduction of sand with plastic fines. *Geotechnical Testing Journal, ASTM*, 36(4):1–9, 2013.

[11] V. Fioravante. Anisotropy of small strain stiffness of Ticino and Kenya sands from seismic wave propagation measured in triaxial testing. *Soils and Foundations*, 40(4):129–142, 2000.

[12] V. Fioravante and R. Capoferri. On the use of multidirectional piezoelectric transducers in triaxial testing. *Geotechnical Testing Journal, ASTM*, 24(3):243–255, 2001.

[13] B.O. Hardin and W.L. Black. Sand stiffness under various triaxial stresses. *Journal of the Soil Mechanics and Foundations Division, ASCE*, 92(SM2):27–42, 1966.

[14] B.O. Hardin and V.P. Drnevich. Shear modulus and damping in soils: measurement and parameter effects. *Journal of the Soil Mechanics and Foundations Division, ASCE*, 98(SM6):603–624, 1972.

[15] B.O. Hardin and M.E. Kalinski. Estimating the shear modulus of gravelly soils. *Journal of Geotechnical and Geoenvironmental Engineering, ASCE*, 131(7):867–875, 2005.

[16] B.O. Hardin and F.E. Richart Jr. Elastic wave velocities in granular soils. *Journal of the Soil Mechanics and Foundations Division, ASCE*, 89(SM1):33–65, 1963.

[17] H. Hertz. Über die Berührung fester elastischer Körper. *Journal reine und angewandte Mathematik*, 92:156–171, 1881.

[18] K. Ishihara. Liquefaction and flow failure during earthquakes. The 33rd Rankine Lecture. *Géotechnique*, 43(3):351–415, 1993.

[19] K. Ishihara. *Soil Behaviour in Earthquake Geotechnics*. Oxford Science Publications, 1996.

[20] T. Iwasaki, F. Tatsuoka, and Y. Takagi. Shear moduli of sands under cyclic torsional shear loading. *Soils and Foundations*, 18(1):39–56, 1978.

[21] F. Jafarzadeh and H. Sadeghi. Experimental study on dynamic properties of sand with emphasis on the degree of saturation. *Soil Dynamics and Earthquake Engineering*, 32:26–41, 2012.

[22] T. Kokusho. Cyclic triaxial test of dynamic soil properties for wide strain range. *Soils and Foundations*, 20(2):45–59, 1980.

[23] S.L. Kramer. *Geotechnical earthquake engineering*. Prentice-Hall, Upper Saddle River, N.J., 1996.

[24] G. Lanzo, M. Vucetic, and M. Doroudian. Reduction of shear modulus at small strains in simple shear. *Journal of Geotechnical and Geoenvironmental Engineering, ASCE*, 123(11):1035–1042, 1997.

[25] X.S. Li and Z.Y. Cai. Effects of low-number previbration cycles on dynamic properties of dry sand. *Journal of Geotechnical and Geoenvironmental Engineering, ASCE*, 125(11):979–987, 1999.

[26] X.S. Li, W.L. Yang, C.K. Chen, and W.C. Wang. Energy-injecting virtual mass resonant column system. *Journal of Geotechnical and Geoenvironmental Engineering, ASCE*, 124(5):428–438, 1998.

[27] D.C.F. Lo Presti, M. Jamiolkowski, O. Pallara, A. Cavallaro, and Pedroni S. Shear modulus and damping of soils. *Géotechnique*, 47(3):603–617, 1997.

[28] D.C.F. Lo Presti, O. Pallara, R. Lancellotta, M. Armandi, and R. Maniscalco. Monotonic and cyclic loading behaviour of two sands at small strains. *Geotechnical Testing Journal, ASTM*, (4):409–424, 1993.

[29] F.-Y. Menq and K.H. Stokoe II. Linear dynamic properties of sandy and gravelly soils from large-scale resonant tests. In Di Benedetto et al., editor, *Deformation Characteristics of Geomaterials*, pages 63–71. Swets & Zeitlinger, Lisse, 2003.

[30] R.D. Mindlin and H. Deresiewicz. Elastic spheres in contact under varying oblique forces. *Journal of Applied Mechanics*, 20:327–344, 1953.

[31] F. Radjai and D.E. Wolf. Features of static pressure in dense granular media. *Granular Matter*, (1):3–8, 1998.

[32] F. Radjai, D.E. Wolf, M. Jean, and J.-J. Moreau. Bimodal character of stress transmission in granular packings. *Physical Review Lett.*, 80(1):61–64, 1998.

[33] R.P. Ray and R.D. Woods. Modulus and damping due to uniform and variable cyclic loading. *Journal of Geotechnical Engineering, ASCE*, 114(8):861–876, 1988.

[34] S.K. Saxena and K.R. Reddy. Dynamic moduli and damping ratios for Monterey No. 0 sand by resonant column tests. *Soils and Foundations*, 29(2):37–51, 1989.

[35] C.K. Shen, X.S. Li, and Y.Z. Gu. Microcomputer based free torsional vibration test. *Journal of Geotechnical Engineering, ASCE*, 111(8):971–986, 1985.

[36] I. Towhata. *Geotechnical Earthquake Engineering*. Springer, 2008.

[37] M. Vucetic. Cyclic threshold shear strains in soils. *Journal of Geotechnical Engineering, ASCE*, 120(12):2208–2228, 1994.

[38] Y.-H. Wang and K.-Y. Tsui. Experimental characterization of dynamic property changes in aged sands. *Journal of Geotechnical and Geoenvironmental Engineering, ASCE*, 135(2):259–270, 2009.

[39] T. Wichtmann, M.A. Navarrete Hernández, and T. Triantafyllidis. On the influence of a non-cohesive content of fines on the small strain stiffness of quartz sand. *Soil Dynamics and Earthquake Engineering*, 69(2):103–114, 2014.

[40] T. Wichtmann, A. Niemunis, and T. Triantafyllidis. Improved simplified calibration procedure for a high-cycle accumulation model. *Soil Dynamics and Earthquake Engineering*, 70(3):118–132, 2015.

[41] T. Wichtmann and T. Triantafyllidis. Influence of the grain size distribution curve of quartz sand on the small strain shear modulus $G_{\max}$. *Journal of Geotechnical and Geoenvironmental Engineering, ASCE*, 135(10):1404–1418, 2009.

[42] T. Wichtmann and T. Triantafyllidis. On the influence of the grain size distribution curve on P-wave velocity, constrained elastic modulus $M_{\max}$ and Poisson's ratio of quartz sands. *Soil Dynamics and Earthquake Engineering*, 30(8):757–766, 2010.

[43] T. Wichtmann and T. Triantafyllidis. Effect of uniformity coefficient on $G/G_{\max}$ and damping ratio of uniform to well graded quartz sands. *Journal of Geotechnical and Geoenvironmental Engineering, ASCE*, 139(1):59–72, 2013.

[44] T. Wichtmann and Th. Triantafyllidis. Über die Korrelation der ödometrischen und der "dynamischen" Steifigkeit nichtbindiger Böden. *Bautechnik*, 83(7):482 – 491, 2006.

[45] T. Wichtmann and Th. Triantafyllidis. Reply to the discussion of T. Benz and P.A. Vermeer on "On the correlation of oedometric and "dynamic" stiffness of non-cohesive soils (Bautechnik 83, No. 7, 2006) (in German). *Bautechnik*, 84(5):364–366, 2007.

[46] T. Wichtmann and Th. Triantafyllidis. On the correlation of "static" and "dynamic" stiffness moduli of non-cohesive soils. *Bautechnik, Special Issue "Geotechnical Engineering", July 2009*, pages 28–39, 2009.

[47] J. Yang and X.Q. Gu. Shear stiffness of granular material at small strains: Does it depend on grain size? *Géotechnique*, 63(2):165–179, 2013.

[48] P. Yu. Discussion of "Moduli and Damping Factors for Dynamic Analyses of Cohesionless Soils" by Seed et al. *Journal of Geotechnical Engineering, ASCE*, 114(8):954–957, 1988.

[49] J. Zhang, R.D. Andrus, and C.H. Juang. Normalized shear modulus and material damping ratio relationships. *Journal of Geotechnical and Geoenvironmental Engineering, ASCE*, 131(4):453–464, 2005.